NJC

ROYAL SOCIETY OF CHEMISTRY

PAPER

View Article Online
View Journal | View Issue

Cite this: *New J. Chem.*, 2024, **48**, 874

On the mechanochemical synthesis of C-scorpionates with an oxime moiety and their application in the copper-catalyzed azide–alkyne cycloaddition (CuAAC) reaction†

Carla Gomes, [a] Mariana Costa,[a] Susana M. M. Lopes, [a] Bernardo Albuquerque Nogueira, [a] Rui Fausto, [ab] José A. Paixão, [c] Teresa M. V. D. Pinho e Melo, [a] Luísa M. D. R. S. Martins [d] and Marta Pineiro *[a]

The development of sustainable processes requires the integration of the principles of green chemistry. In this work, we develop the solvent-free synthesis of bis- and tris-(pyrazol-1-yl)methanes from pyrazole and halooximes *via* 1,4-addition to conjugated α-halogenated nitrosoalkenes generated *in situ* under ball milling. The pro-ligands were complexed with copper, using a solvent-free procedure with equimolar quantities of reactants, to give catalysts copper(II) C-scorpionates with the oxime substituent at the C-center. The new catalysts were used to efficiently catalyze azide–alkyne cycloaddition reactions under solvent-free mechanochemical conditions. Through the overall process, we combine atom economy, the use of safer solvents and auxiliaries, design for energy efficiency and reduction of derivatives and catalysis (the 1st, 5th, 6th, 8th, and 9th principles of Green Chemistry). The sustainability metrics show that mechanochemistry provides a greener and more sustainable approach for the preparation of the catalysts and for the copper-catalyzed azide–alkyne cycloaddition (CuAAC) reactions. The development of novel C-scorpionates and their metal complexes, and their subsequent application in CuAAC reactions under mechanochemical conditions, presents an exciting avenue for the future of sustainable click chemistry.

Received 31st October 2023,
Accepted 30th November 2023

DOI: 10.1039/d3nj05017c

rsc.li/njc

1. Introduction

Mechanochemistry involves physicochemical transformations driven by mechanical energy originating from compression, shear, impact, *etc*. These reactions have been known since ancient times, and their ability to promote the reaction under solvent-free conditions has attracted the attention of contemporary synthetic chemists seeking for sustainable synthetic processes. Mechanochemistry has become a consolidated alternative tool for synthesis.[1]

The copper-catalyzed azide–alkyne cycloaddition (CuAAC) reaction yielding triazoles is a widely used metal catalyzed reaction and a truly "*click reaction*". The unique features of the CuAAC reaction, including its biorthogonality, high regioselectivity and its characteristics in line with the requirements of green chemistry,[2–4] make it a popular choice for applications in diverse fields, such as medicinal and polymer chemistries, as well as materials and nanomaterials science. This was publicly recognized with the award of Nobel Prize in Chemistry to Morten Meldal, Carolyn R. Bertozzi and K. Barry Sharpless in 2022.[5–8] Researchers in this area have focused on developing more sustainable conditions by seeking greener solvents and copper precursors that can generate copper(I) efficiently, while decreasing or eliminating the need for reducing agents and bases.

Mechanochemical click CuAAC reactions enable the preparation of triazoles in good yields and with high regioselectivity under solvent-free conditions, using diverse catalytic systems. Applying $Cu(OAc)_2$ as the copper source, sodium ascorbate as the reducing agent, and SiO_2 as the grinding auxiliary in a planetary ball mill, triazoles were obtained in good yields, with almost no side products and in a short reaction time (~10 min).[9] Other studies carried out using a mixer milling system showed moderate yields of quinolines containing the phenyl-1,2,3-triazole unit when $Cu(OAc)_2$ was used as a

[a] *CQC-IMS and Department of Chemistry, University of Coimbra, 3004-535, Coimbra, Portugal. E-mail: mpineiro@qui.uc.pt*
[b] *Faculty of Sciences and Letters, Department of Physics, Istanbul Kultur University, Ataköy Campus, Bakirköy 34156, Istanbul, Turkey*
[c] *CFisUC and Department of Physics, University of Coimbra, 3004-516 Coimbra, Portugal*
[d] *Centro de Química Estrutural, Institute of Molecular Sciences, Departamento de Engenharia Química, Instituto Superior Técnico, Universidade de Lisboa, Av. Rovisco Pais 1, 1049-001 Lisboa, Portugal*

† Electronic supplementary information (ESI) available. CCDC 2096452. For ESI and crystallographic data in CIF or other electronic format see DOI: **https://doi.org/10.1039/d3nj05017c**

catalyst without any reducing agent. Using the same type of milling, the reaction yield increased when copper(I) was used as a catalyst in the presence of a tertiary amine, and when milling vessels and balls of brass (an alloy of copper and zinc) were used as catalysts, with *N*,*N*-di-isopropylethylamine (DIPEA), together with a small amount of acetic acid as auxiliaries.[10] Furthermore, copper powder was also selected as a catalyst for the reaction between benzyl azides and alkynes under planetary ball milling.[11] In copper vials as reaction containers, the catalyzed reaction between aryl and alkyl alkynes, benzyl bromine, and sodium azide afforded target triazoles, although longer reaction times were required.[12] This study also allowed concluding on the safety of manipulating sodium azide under mechanochemical conditions (high-energy milling conditions), highlighting that azide reactions under mechanochemical conditions are indeed much safer than when conducted through traditional solution-based chemistry in a glass apparatus.[12] Propargyl glycoside derivatives were also shown to be efficiently coupled with azides,[13] by using $CuSO_4$/sodium ascorbate and *t*BuOH/H_2O, while applying similar experimental conditions, the preparation of cancer cell targeting polyethylene glycol-functionalized nanographene oxide was reported,[14] pointing out the capability of mechanochemistry to solve the problem of promoting the reaction between reactants with different solubilities.

N-ligands protect copper(I) from oxidation, by modulating the redox potential of the Cu(II)/Cu(I) pair, and they influence the solvation energy of copper ions and also act as a base to promote the initial formation of copper(I) acetylide, thus increasing the CuAAC reaction rate. Monodentate N-ligands (amines) and polydentate N-ligands, such as 1,1,4,7,7-pentamethyldiethylenetriamine (PMDETA), significantly accelerate the CuAAC reaction.[5]

Tris(pyrazol-1-yl)methanes, also known as C-scorpionates, are among the most versatile classes of N-heterocyclic ligands,[15–20] however the application of their copper complexes as catalysts for the CuAAC reaction is scarce. To the best of our knowledge, only two examples of such use of the copper complexes of C-scorpionates have been reported hitherto. Cano and co-workers used copper(I) C-scorpionates to efficiently promote the formation of *N*-sulfonyl-1,2,3-triazoles from sulfonylazides and alkynes in chloroform, at 40 °C for 24 h,[21] while Mahmoud and co-workers used copper(I) C-scorpionates and copper(II) C-scorpionates as catalysts for the three-component CuAAC reaction in aqueous medium, under microwave irradiation, at 125 °C for 30 min.[22]

Having in mind the development of genuine sustainable processes, in the present investigation we explored the utilization of mechanochemistry for the synthesis of a novel class of C-scorpionates and of their metal complexes, and the subsequent application of the new Cu(II) complexes in click chemistry, in particular in the multicomponent CuAAC reaction, under mechanochemical conditions, to afford triazoles.

2. Results and discussion

2.1. Synthesis and structural characterization of novel C-scorpionates

The synthesis of tris(pyrazol-1-yl)methanes featuring an oxime group at the C-center was achieved previously using a solution-based approach by the 1,4-addition of pyrazoles to conjugated α-halogenated nitrosoalkenes.[23] To develop and optimize the mechanochemical synthesis of these compounds under high-speed ball milling conditions, the synthesis of 2,2,2-tris(1*H*-pyrazol-1-yl)acetaldehyde oxime (**3a**) was used as the model reaction (Scheme 1).

To obtain the desired compound, **3a**, as depicted in Scheme 1, equivalent amounts of oxime **2**, synthesized using a previously described methodology,[23] pyrazole (**1a**) and sodium carbonate were mixed in a stainless steel jar under ball milling conditions. Specifically, high-speed vibrations at 20 Hz for 30 min with two stainless steel balls (7 mm of diameter) were utilized. Using this approach, 33% yield of the desired complex was obtained (entry 1, Table 1). By increasing the milling frequency to 25 Hz, the reaction yield reached 52% (entry 2, Table 1). However, increasing the milling frequency (up to 30 Hz), the number of milling balls, or extended reaction times did not improve the reaction yield (entries 3 to 5, Table 1). Interestingly, the order in which reactants were added to the milling jar was found to have a notable influence on the reaction outcome. It was observed that sodium carbonate should be added on top of pyrazole. Adding it on top of the oxime resulted in the immediate onset of the elimination reaction, with the formation of HCl, which led to the depletion of the reactant and subsequent dropping of the reaction yield to only 12% (entry 6, Table 1).

The optimization of reaction conditions under mechanical action allowed to obtain the desired compound in 52% yield, after ball milling at 25 Hz during 30 min (see Scheme 1). The elimination of dichloromethane (use restricted in accordance with the European directive[24]) as well as the reduction of the reaction time from 16 h to 30 min is in line with the concerns for the development of more sustainable processes. According to previous studies, in solution, the reaction mechanism is highly dependent on both the basicity of the N-heterocycle and the nature of the oxime.[25] In the case of the reaction of pyrazole and 2,2,2-trichloroacetaldehyde oxime to afford tris(pyrazol-1-yl)methane, the proposed mechanism consists of three

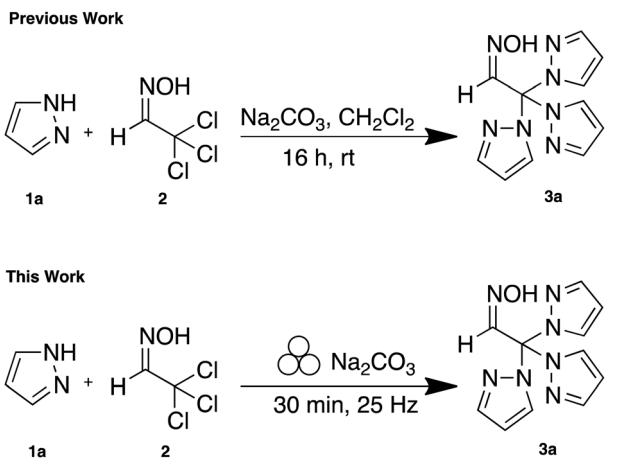

Scheme 1 Strategies for the synthesis of tris(pyrazol-1-yl)methane featuring an oxime group at the C-center.

Table 1 Optimization of the conditions for the synthesis of tris(pyrazol-1-yl)methanes bearing an oxime group at the central carbon (data for the selected model reaction yielding **3a**)

Mechanochemistry conditions				
Entry	Frequency (Hz)	Number of balls	Time (min)	Yield[a] (%)
1	20	2	30	33[b]
2	25	2	30	52[b]
3	30	2	30	51[b]
4	25	2	60	52[b]
5	25	3	30	49[b]
6	25	2	30	12[c]

[a] Isolated yields after column chromatography [eluent: AcOEt/hexane (2 : 1)]. [b] Order of addition of the reactants: oxime, pyrazole and then sodium carbonate. [c] Order of addition of the reactants: oxime, sodium carbonate and then pyrazole.

consecutive conjugated addition reactions (Michael addition) of pyrazole to the *in situ* generated nitrosoalkenes.

The X-ray analysis of the crystals of **3a** obtained after the recrystallization of the reaction product synthesized under mechanical action in ethanol (Fig. 1) clearly established that the (*E*)-oxime was obtained exclusively. The ^{1}H-NMR spectrum of the reaction product (ESI,† Fig. S7) shows only one peak at 11.98 ppm, *i.e.*, at the typical region of the proton of an oxime group with *E* configuration.[26] The *E* configuration was not evident in the bidimensional NOESY spectrum (ESI,† Fig. S8).

The performed single-crystal X-ray crystallography study unambiguously confirmed that the *E* configuration is adopted by **3a** in the crystalline state, as depicted in the ORTEP graph shown in Fig. 1 (left). All H-atoms could be located using the difference electron density maps. The compound crystallizes in the centrosymmetric monoclinic space group $P2_1/n$ with cell parameters a = 10.2989(3)Å, b = 9.5354(3) Å, c = 12.3745(4) Å, α = 90°, β = 91.395(2)°, and γ = 90°. Valence angles and bond lengths are unexceptional, with average values Nsp^2–Nsp^2 [1.355(2) Å], Csp^2–Nsp^2 [1.32(5) Å], Nsp^2–Csp^3 [1.453(4) Å], Csp^3–Csp^2 [1.5159(2) Å], Csp^3–Csp^3 [1.37(2) Å], Nsp^2–O [1.3906(14) Å]. The acetaldehyde oxime group is nearly planar, as shown by the torsion angle O1–N1–C2–C1 [178.99(10)°]. There is a small but significant deviation from the ideal tetrahedral geometry around C1, with valence angles N2–C1–N6 [107.92(9)°], N4–C1–N6 [108.91(9)°], N4–C1–N2 [107.85(9)°], N2–C1–C2 [108.91(9)°] N4–C1–C2 [110.38(9)°] and N6–C1–C2 [112.72(10)°]. The three pyrazole rings are planar with the rms deviation of the atoms from the least squares planes not exceeding 0.006 Å. The rings adopt a propeller-like conformation as shown by angles ∠(N2–N3–C3–C4–C5/N4–N5–C6–C7–C8) [88.06(5)°], ∠(N2–N3–C3–C4–C5/N6–N7–C9–C10–11) [81.39(6)°], ∠(N4–N5–C6–C7–C8/N6–N7–C9–C10–C11) [79.28(6)°] and depicted in Fig. 1 (center). The torsion angle N1–C2–C1–N2 [166.71(11)°] shows that the aldoxime group is rotated by 13° from the ideal bisecting position arising from a rotation around the single C1–C2 bond likely caused by a combination of steric effects and the involvement of O1 in intermolecular hydrogen bonding.

The main synthon occurring in the crystal structure is a pair of molecules related by an inversion center, linked by a bifurcated hydrogen bond, as shown in Fig. 1 (right). The donated hydroxyl proton is shared towards the lone pairs of two bare N atoms of the symmetry-related molecule, one belonging to the nearest pyrazole rings, and the other being the N atom of the oxime group, with geometry O1–H1···N1^i [i = 1 − x, 1 − y, 1 − z; D–H 0.961(19); H···A: 2.190(19) Å; D···A: 3.0044(14) Å; ∠D–H–A: 141.7(15)°]; O1–H1···N7^i [i = 1 − x, 1 − y, 1 − z; D–H 0.961(19); H···A: 2.162(18) Å; D···A: 2.9274(15) Å; ∠D–H–A: 135.7(14)°]. These pairs of molecules are further interconnected in a 3D network by weaker interactions of the C–H···N type involving the remaining two bare N atoms of the pyrazole rings. The packing is compact and there are no sizeable voids in the crystal structure accessible to solvent molecules. For the XRD see Tables S10–S22 in the ESI.†

The infrared (IR) and Raman spectra of the synthesized ligand **3a** are presented in Fig. 2, together with the corresponding calculated spectra (B3LYP/6-311++G(d,p), scaled as described in the Experimental section – computational details). The theoretical spectra were calculated after the optimization of the dimeric structure present in the crystal of the compound, using the crystallographic data as initial geometry.

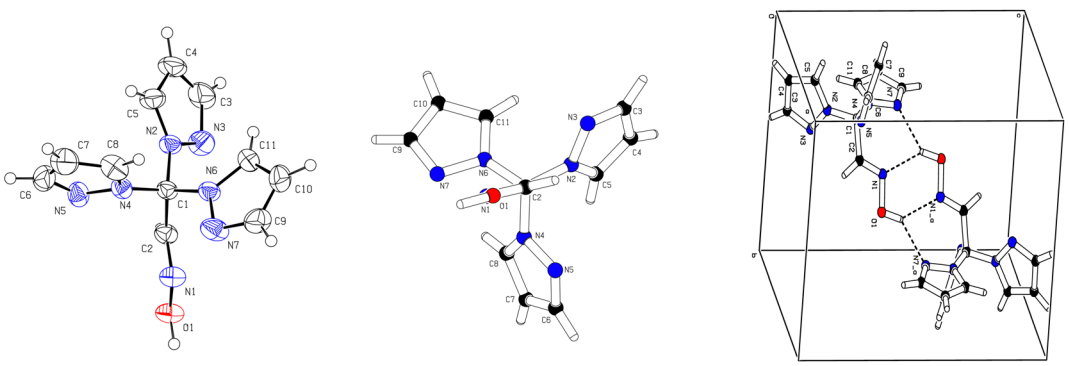

Fig. 1 Left: ORTEP plot of the molecule depicting the displacement ellipsoids (drawn at the 50% probability level), showing the adopted atom numbering scheme; centre: molecule configuration viewed along the C1–C2 bond, showing the propeller-like arrangement of the rings; right: the unit cell with the dimeric synthon of the crystal structure, consisting of a pair of molecules related by an inversion centre, interconnected by a bifurcated O–H···N bond.

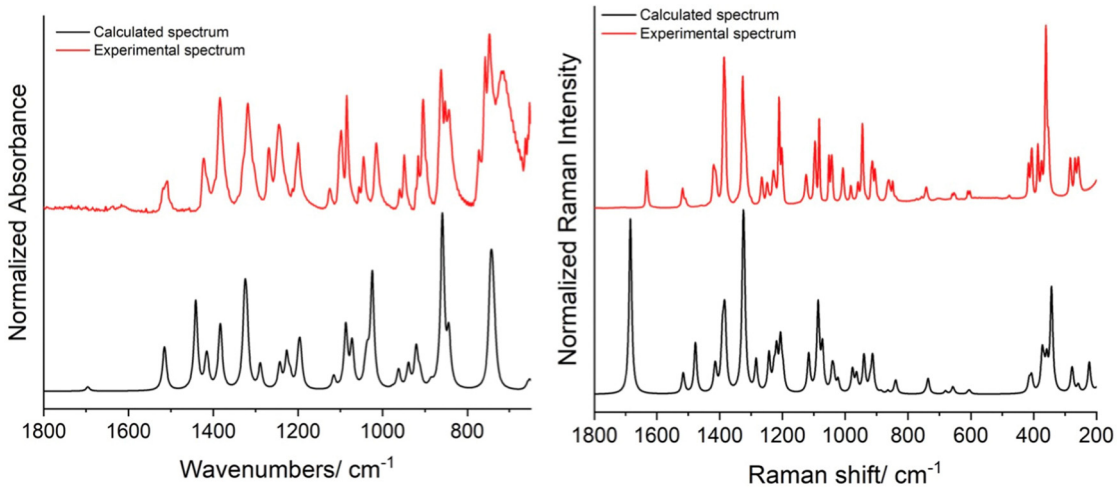

Fig. 2 Calculated (B3LYP/6-311++G(d,p), scaled) and experimental (ATR mode) IR spectra (left) and calculated (B3LYP/6-311++G(d,p), scaled) and experimental Raman spectra (right) of (*E*)-2,2,2-tris(1*H*-pyrazol-1-yl)acetaldehyde oxime **3a**.

As shown in Fig. 2, the calculated and experimental spectra exhibited a remarkable resemblance, with the major spectral features observed experimentally being well reproduced by the calculations (for assignments, see the ESI,† Table S1). This fact should be highlighted, because the calculations were undertaken considering only the isolated dimeric structural unit of the compound, allowing to conclude that the inter-dimer interactions in the crystal are weak enough not to disturb extensively the intra-dimer vibrational potential. The general good reproducibility of the experimental spectra of the studied model ligand **3a** by the calculations also suggested the possibility to use successfully vibrational data obtained theoretically to help to undertake the general structural characterization of the complexes of the oxime ligand investigated in the present study, as demonstrated in Section 2.2.

Besides the chosen model ligand **3a**, other oxime derivatives of tris(pyrazolyl)methanes and bis(pyrazol-1-yl)methanes were synthesized *via* mechanochemistry in the present investigation (see Scheme 2, where the optimized conditions for the synthesis are also provided). The reproducibility of the synthetic methods using mechanochemistry is high. For example, the synthesis of ligand **3a** yielded 52, 53 and 50% in three independent experiments. It is interesting to point out that the yields of the mechanochemical syntheses performed using oximes from aldehydes were significantly higher than those obtained using oximes derived from ketones, thus following the same trend observed for the corresponding reactions in solution.[23]

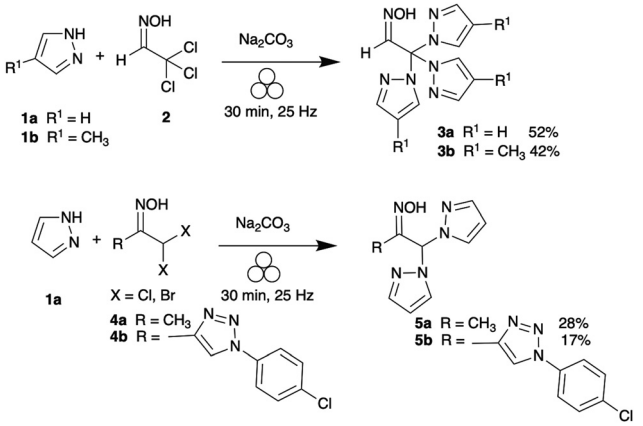

Scheme 2 Synthesis of tris(pyrazol-1-yl)methanes and bis(pyrazol-1-yl)methanes under mechanical action and the corresponding reaction yields. The precursor oximes, 1,1-dichloropropano-2-one oxime (**4a**) and 1-(1-*p*-chlorophenyl-1*H*-1,2,3-triazol-4-yl)-2,2-dibromoethanone oxime (**4b**), were prepared using a methodology described previously[27] and through α-bromination with Br_2/HOAc of 1-(1-*p*-chlorophenyl-1*H*-1,2,3-triazol-4-yl)ethanone[28] followed by oximation with hydroxylamine hydrochloride in ethanol (yield: 81%), respectively (see structural characterization in the ESI,† Fig. S1–S6).

2.2. Copper(II) C-scorpionates synthesis and characterization

Two model copper(II) C-scorpionate complexes of the (*E*)-2,2,2-tris(1*H*-pyrazol-1-yl)acetaldehyde oxime (**3a**) were synthesised *via* mechanochemistry (complexes **6a** and **6b**; Scheme 3). The complexation was successfully achieved using a stoichiometric amount of copper salt (copper chloride dihydrate or copper acetate monohydrated) under mechanical action during 30 min at 25 Hz in a stainless-steel jar using two stainless steel balls (7 mm). Complexes **6a** and **6b** were obtained in 86% and 79% yields, respectively.

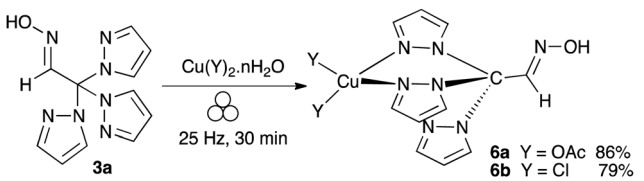

Scheme 3 Mechanochemical synthesis of copper complexes **6a** and **6b** of (*E*)-2,2,2-tris(1*H*-pyrazol-1-yl)acetaldehyde oxime (**3a**).

For comparison, the two model copper complexes were also synthesized in solution, following the general procedure described.[29] The melting points of the complexes prepared under ball milling and in solution were found to be similar (151.7–152.6 °C and 151.9–152.6 °C, respectively, in the case of **6a**, and 118.9–119.5 °C and 118.5–119.0 °C, respectively, for **6b**). The high-resolution mass spectrum (HRMS) of **6a** shows a peak at m/z = 379.0446, corresponding to the loss of an acetate group, and the elemental analysis data match the molecular formula $C_{15}H_{17}CuN_7O_5 + H_2O$. For copper complex **6b**, the high-resolution mass spectrum shows a peak at m/z = 390.977, which matches the molecular formula $C_{11}H_{11}CuCl_2N_7O$, and the elemental analysis correlates with the formula $C_{11}H_{11}CuN_7OCl_2 + H_2O$.

Owing to the impossibility to obtain ^{1}H-NMR spectra due to the paramagnetic nature of the copper(II) complexes, we endeavoured to acquire high-quality crystals of the synthesized complexes for the determination of their single crystal X-ray structure. Regrettably, our efforts proved unsuccessful. Consequently, we resorted to IR and Raman spectroscopies to investigate the structure of the copper complexes. The analysis of the experimental spectroscopic data was supported by the theoretical prediction of the vibrational spectra of the complexes (see the Experimental section for details).

The structures of the isolated molecule of the ligand and of complexes **6a** and **6b** were first investigated using quantum chemical calculations performed at the DFT(B3LYP)/6-311++G-(d,p) level. The optimized structure of the ligand (Fig. 3, left) closely resembles that observed experimentally in crystalline phase (Fig. 1), with the aldoxime group being almost planar (O1–N1–C2–C1 torsion angle = 179.9°). There is also a deviation from the tetrahedral geometry around the C1 atom predicted by the calculation that is comparable to that found in the crystal, with the calculated N2–C1–N6, N4–C1–N6, N4–C1–N2, N2–C1–C2, N4–C1–C2 and N6–C1–C2 angles presenting values in the range 107.7–114.1°. Additionally, also in agreement with the crystallographic data, the calculations predict the plane of the oxime group slightly deviated (by ~9.0°, as defined by the N1–C2–C1–N2 torsion angle) from the plane that bisects perpendicularly the angle N4–C1–N6.

In the optimized structures of complexes **6a** and **6b** (Fig. 3), the calculated bond angles and dihedral angles of the oxime ligand exhibit values similar to those found for the free ligand. The N1–C2–C1–N2 torsion, which represents the deviation from the plane that bisects perpendicularly the angle N4–C1–N6, is equal to 10.8° in both complexes **6a** and **6b**. On the other hand, the angles formed between the pyrazole rings and the oxime moiety plane differ in the two complexes and in the free ligand (see Fig. 3). In the free ligand, the orientation of the rings (as defined by the dihedral angles C2–C1–N2–N3, C2–C1–N4–N5 and C2–C1–N6–N7) confers the structure a propeller-like arrangement, with dihedral angles equal to 40.5, 42.2 and 63.8°, respectively. In the predicted structure of the **6a** complex, the corresponding values of these dihedral angles are 70.2°, 174.1° and 164.4°, while in that of complex **6b**, these dihedral angles are 72.2°, 172.1° and 172.2°, respectively. As shown in Fig. 3, this means that in complexes **6a** and **6b**, two of the pyrazole rings (rings 2 and 3) are oriented in such a way that their bare nitrogen atom (N5 and N7) faces the copper atom, while ring 1 is oriented resembling the correspondent ring in the free ligand structure.

The theoretical IR and Raman spectra of complexes **6a** and **6b** were obtained for the optimized structures and were compared with the corresponding calculated spectrum of pro-ligand **3a** (Fig. 4). Both calculated Raman and IR spectra of the complexes present noticeable differences compared to the computed spectra of the ligand, some of which are highlighted in Fig. 4 by labelling the bands with the corresponding maximum intensity wavenumber. The tentative assignment of the major features of the experimental and calculated spectra of **6a** and **6b** is provided in the ESI,† Tables S2 and S3, respectively.

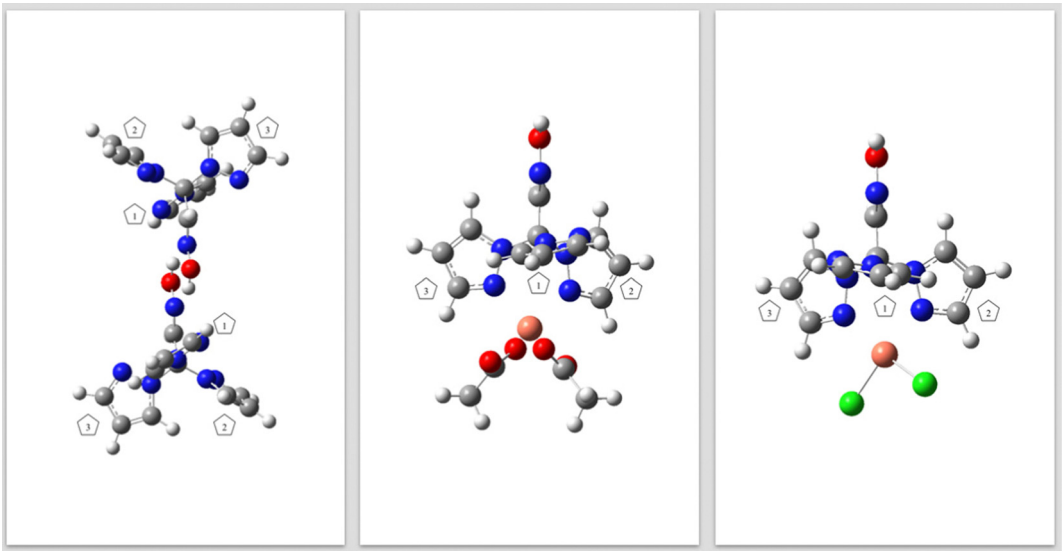

Fig. 3 Optimized DFT(B3LYP)/6-311++G(d,p) calculated structures for pro-ligand **3** (left) and copper complexes **6a** (centre) and **6b** (right).

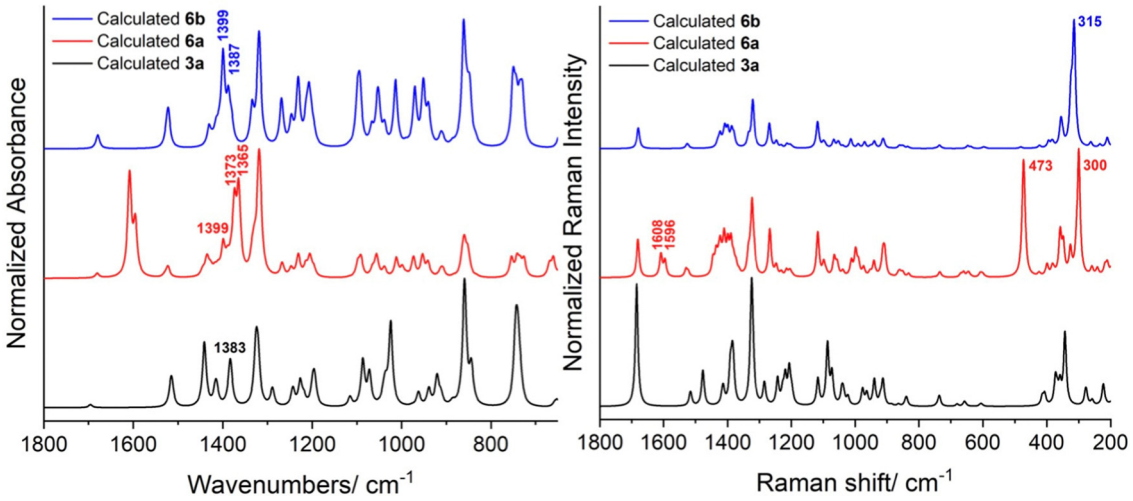

Fig. 4 Comparison between the IR (left) and Raman (right) scaled calculated spectra of the pro-ligand **3a** and the complexes **6a** and **6b**, obtained at the B3LYP/6-311++G(d,p) level of theory.

As expected, the calculated Raman spectra of the complexes present several intense additional bands, compared to the spectrum of the C-scorpionate pro-ligand. In the case of **6a**, these bands are mainly due to the presence of the complex of the acetate (OAc) ligands, such as those predicted at 300 cm^{-1} (corresponding to the Cu–OAc stretching mode), 473 cm^{-1} (C–C bending mode of OAc) and 1596/1608 cm^{-1} (C═O stretching of OAc). These bands can then be expected to be possible marker bands for this complex. On the other hand, the calculated Raman spectrum of complex **6b** presents its highest intensity band at 315 cm^{-1}, which is ascribable to the Cu–Cl stretching vibration and, thus, also appears as a possible marker band for this complex.

The calculated IR spectra of the isolated C-scorpionate pro-ligand and those of the two complexes are in general more similar to each other than the corresponding Raman spectra (excluding the C═O stretching modes of OAc in **6a**, in the 1595–1610 cm^{-1} region). However, in the range of 1350–1405 cm^{-1}, it is also possible to observe some noticeable spectral differences in the IR spectra. While in the ligand spectrum, only one band is present (1383 cm^{-1}, OH bending vibration), in the spectrum of **6a**, there are bands at 1365 (OAc CH_3 rocking mode), 1373 (OAc C–C stretching vibration) and at 1399 cm^{-1} (OH bending vibration), and in the spectrum of complex **6b**, bands are observed at 1387 and at 1399 cm^{-1}, which are assigned to the CH (aromatic) and OH bending modes, respectively.

Fig. 5 compares the experimental spectra (both IR and Raman) of ligand **3a** and of complexes **6a** and **6b**, obtained under ball milling (the same comparison, with the spectra of the complexes obtained in solution is presented in Fig. S19, in the ESI†). The above highlighted marker bands of the **6a** and **6b** complexes, identified based on their calculated spectra, are, as expected, clearly visible in their experimental spectra (compare

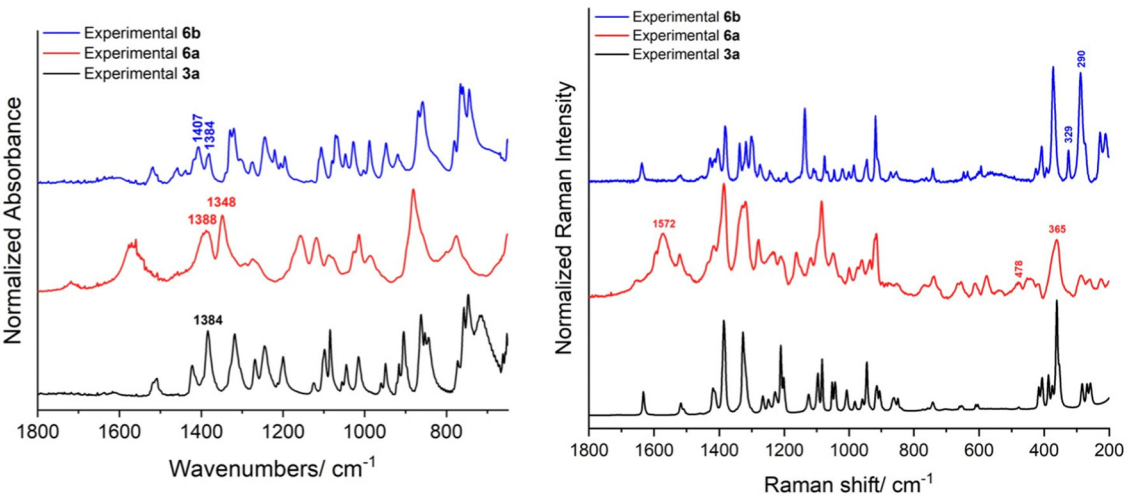

Fig. 5 Comparison between the IR (left) and Raman (right) experimental spectra of pro-ligand **3a** and complexes **6a** and **6b**, obtained under ball milling.

Fig. 4, 5 and Fig. S19 in the ESI†). In the Raman experimental spectrum of complex **6a**, the Cu–OAc stretching mode appears at 365 cm^{-1}, and the C–C bending vibration and C═O stretching modes of the OAc ligands give rise to bands at 478 cm^{-1} and 1572 cm^{-1} (single broad band), respectively, in good correspondence with the theoretically predicted spectrum. In the case of **6b**, the Cu–Cl stretching marker band vibration is observed in the experimental spectrum at 290 and 329 cm^{-1} (calculated: 315 cm^{-1}), respectively. The appearance of the two bands due to the Cu–Cl stretching mode in the experimental spectra (for both the spectra of the complex obtained using mechanochemical and conventional procedures, see Fig. 5 and Fig. S19, ESI†) might indicate that the two chlorine atoms have different positions relative to the metal atom in the complex, with one being more tightly bonded than the other. In the case of the IR spectra, the above-mentioned identified theoretical marker bands for the ligand and the complexes in the 1350–1405 cm^{-1} spectral range are observed in the experimental spectra of the ligand at 1384 cm^{-1}, at 1365 and 1388 cm^{-1} for complex **6a** (the latter being a broad band comprising both the OAc C–C stretching vibration and the OH bending mode), and at 1384 and 1407 cm^{-1} for complex **6b**, showing very good correspondence with the predicted frequency values.

The resemblance of the experimental spectra obtained for the complexes obtained under ball milling and from the solution (compare Fig. 5 and Fig. S19 in the ESI†) is highlighted. The few noticeable spectral differences might be attributed to the different crystalline/amorphous phases (or degree of crystallinity) resulting from the two complexation procedures.

Following the success in preparing the C-scorpionate complexes **6a** and **6b**, a set of other copper complexes of triazole-oxime ligands was prepared, using the above described mechanochemistry methodology, in high yields (Chart 1; characterization provided in the ESI†).

2.3. Azide–alkyne cycloaddition (AAC) catalyzed reaction

The three-component AAC reaction carried out using 3-butynol, benzyl bromide and sodium azide was used as the model reaction to explore the catalytic activity of the synthetized copper(II) C-scorpionates (Scheme 4).

Ball milling was applied for all the catalyzed reactions, using equimolar amounts of the three reactants in stainless steel jars with two stainless steel balls (7 mm) and a frequency vibration of 30 Hz. Ball milling of the three reactants under the above described conditions for 3 h did not result in any reaction product, indicating that the metal in stainless steel jars and balls cannot catalyze the reaction (entry 1, Table 3). Nonetheless, the use of 1.5 mol% (relative to alkyne) of copper acetate monohydrate as the catalyst led to the reaction product in 37% yield, after isolation and purification through column chromatography (entry 2, Table 3). This result highlights the crucial role of copper as a catalyst, and the mechanochemical action leads to the formation of catalytic Cu(I) species due to the reduction of $Cu(OAc)_2$ in the presence of sodium azide (**12**), benzyl bromide (**11**) and the alkyne (**10**). Moreover, the reduction of Cu(II) was promoted under ball milling conditions through the Glaser reaction[30–33] without requiring reducing agents, additional bases or water.

To determine the influence of basicity of the oxime group [pK_a (aldoxime) = 28.5, Bordwell pK_a Table[34]] in the catalytic cycle, the reaction was performed adding copper acetate and ligand **3a** to the azide/alkyne/benzyl mixture. After milling for 90 min under the above conditions, 1,2,3-triazole **13** was obtained in 33% yield (entry 3, Table 2), proving that the basicity of the oxime does not influence the reaction.

When 1.5 mol% (relative to alkyne) of copper C-scorpionate **6a** was used as a catalyst, the triazole was obtained in 78% yield (entry 4, Table 2), pointing out the capability of the copper C-scorpionate as a catalyst and its ability to increase the reaction rate.

Martins and co-workers have successfully used copper(I) scorpionates and copper(II) scorpionates as catalysts for the

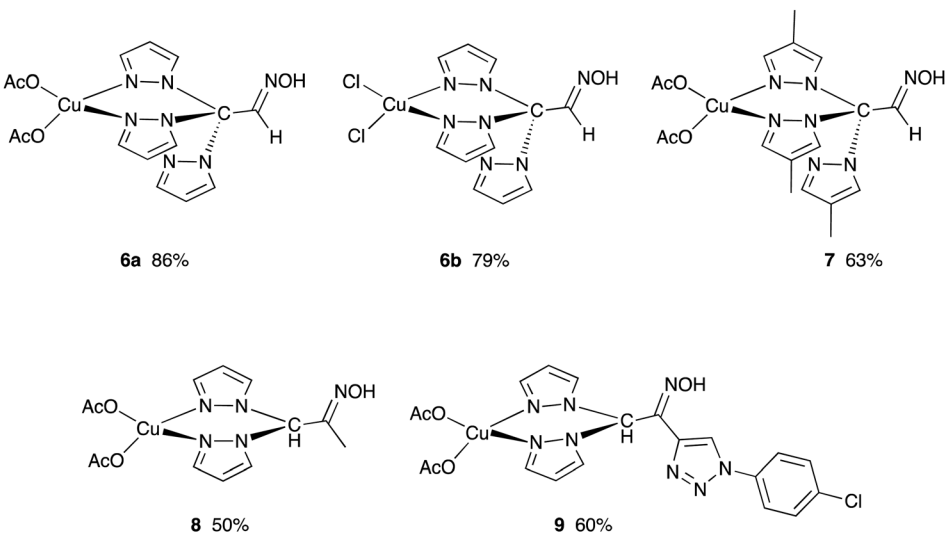

6a 86% **6b** 79% **7** 63%

8 50% **9** 60%

Chart 1 Copper complexes synthetized under ball milling at 25 Hz for 30 min.

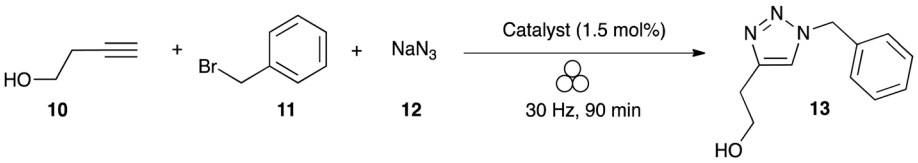

Scheme 4 Three-component AAC reaction of 3-butynol (**10**), benzyl bromide (**11**) and sodium azide (**12**) used as the model reaction.

three-component CuAAC reaction under microwave irradiation.[22] In that study, it was observed that under similar reaction conditions (solvent: H_2O/MeOH (1 : 1), MW, 125 °C, 30 min) but using **6a** as the catalyst, triazole 2-(1-benzyl-1*H*-1,2,3-triazol-4-yl)ethanol was obtained in 64% yield (entry 5, Table 2). Knowing the effect that oxidizable alcohols and water could have in the reduction of Cu(II), a H_2O/MeOH (1 : 1) mixture was chosen to perform the reaction under liquid-assisted mechanochemistry conditions. Using 15 μL of H_2O/MeOH (1 : 1) and milling for 90 min at 30 Hz, the desired triazole **13** was obtained in 53% yield (entry 6, Table 2), indicating that neither water nor methanol has influence on the catalytic cycle, reinforcing the oxidative homocoupling of terminal alkynes as the main mechanism to form the active Cu(I) catalytic species.

Although acetate was previously described as a co-ligand with a good compromise between basicity and non-nucleophilicity, favoring metalation of the terminal alkyne without disfavoring the formation of the dinuclear intermediate and being very efficient for the protodemetallation step,[35] the C-scorpionate complex **6b** was tested as a catalyst of the reaction model (Scheme 4). The substitution of acetate by chloride resulted in a significant decrease in reaction yield, dropping to 49%. The methyl group at the C-4 of pyrazole also decreased the efficiency of the catalyst (entry 8, Table 2). The copper complex of the unsubstituted bis-pyrazole oxime ligand was found to produce good reaction yields (entry 9, Table 2), while the presence of the triazole unit at the C-scorpionate, complex **9**, decreases the yield of the catalyzed reaction (entry 10, Table 2). The results show the influence of the structure of the ligand in the complex catalytic activity, where the increase of the size of the pro-ligand leads to a decrease in the activity, while the presence of unsubstituted pyrazole units leads to higher yields of triazole.

The CuAAC reaction under ball milling using the best reaction conditions (entry 4, Table 2) was further studied by carrying out the formal cycloaddition using aliphatic and aromatic alkynes, leading to triazole derivatives **13–18** in good yields, (Chart 2, see Fig. S20–S25 in the ESI† for structural characterization data).

2.4. Sustainability assessment

Mechanochemistry offers a solvent-free approach for synthesizing tris- and bis-pyrazole compounds with the oxime substituent at the central C atom, complexing them with copper, and utilizing them as catalysts for the solvent-free three-component azide–alkyne cycloaddition reaction. To evaluate the sustainability of the developed processes, three sustainability metrics – atom economy,[36] *E*-Factor[37] and EcoScale[38] – were applied to the model reactions, as shown in Fig. 6.

Atom economy is determined using the chemical equation and is independent of experimental reaction conditions. While the ligand synthesis shows modest atom economy due to the use of 3 equivalents of sodium carbonate, the complexation reaction and the CuAAC reaction exhibit almost perfect and high atom economy, respectively (Fig. 6).

The values obtained for the *E*-factor and the EcoScale are presented in Table 3. The data used to estimate both metrics are presented in the ESI† (Tables S4–S7). For comparison, previously described methods for the synthesis of the same compounds or structurally similar compounds (in the case of the new compounds) were chosen.

The *E*-factor is the ratio of the mass of waste per mass of product: *E*-factor = (total mass of waste/mass of the product). Therefore, the lower the value, the more sustainable the process can be considered. The EcoScale is a post-synthetic tool that evaluates other aspects of the synthetic process, namely, toxicity of the reactants, energy input (time and temperature of the reaction) and procedure safety (see Table S4 in the ESI†). All the procedures to be analyzed start with 100 points, and the points are subtracted as each of the evaluated parameters deviates

Table 2 Reaction conditions of 3-butinol/benzyl bromide/sodium azide (1 : 1 : 1), 1.5 mol% catalyst

Entry	Catalyst	Reaction conditions	Yield (%)
1	—	Ball milling 30 Hz, 3 h	0
2	$Cu(OAc)_2{\cdot}H_2O$	Ball milling 30 Hz, 90 min	37
3	$Cu(OAc)_2{\cdot}H_2O$ + **3a**	Ball milling 30 Hz, 90 min	33
4	**6a**	Ball milling 30 Hz, 90 min	78
5	**6a**	H_2O/MeOH MW (125 °C, 30 min)	64
6	**6a**	LAG (H_2O/MeOH) Ball milling 30 Hz, 90 min	53
7	**6b**	Ball milling 30 Hz, 90 min	49
8	**7**	Ball milling 30 Hz, 90 min	59
9	**8**	Ball milling 30 Hz, 90 min	68
10	**9**	Ball milling 30 Hz, 90 min	55

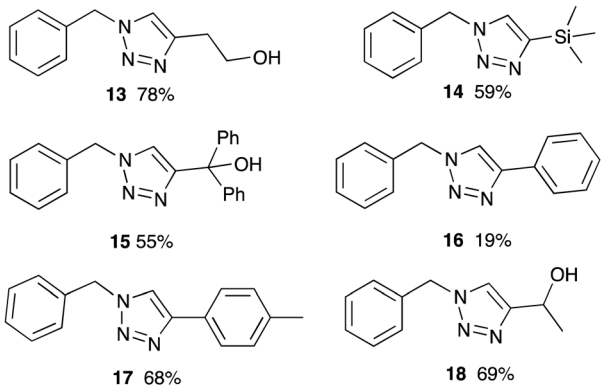

Chart 2 Triazoles obtained through the CuAAC reaction under ball milling conditions.

from the ideal of sustainability. Therefore, the higher the value, the more sustainable the process will be.

The synthesis of the pro-ligands, and therefore of the catalyst, requires the prior preparation of trichloroacetaldehyde oxime. The latter was prepared under conventional conditions following a known procedure. The *E*-factor of this reaction is 6, a good ratio of waste/product, and the EcoScale is 47.5, (ESI,† Table S5) a moderate value, far from the 100 points ideals for this metric, mostly due to safety issues of the reactants used.

The synthesis of tris-pyrazole ligands under free-solvent ball milling conditions (this work) yields the desired compound in lower yield than the synthesis in solution, using dichloromethane as a solvent as described by Pinho e Melo *et al.*[23] However, the *E*-factor for the mechanochemical transformation (*E*-Factor = 6) is ten times lower than that obtained for the synthesis in solution (*E*-Factor = 68), which reflects the influence of the mass of solvent in the reaction waste. The almost equal EcoScale values achieved for both methods (51.5 and 46.5 for mechanochemical and solution method, respectively) show that the decrease of the reaction yield under ball milling is compensated from the point of view of sustainability by the elimination of the chlorinated solvent (ESI,† Table S6).

Table 3 Reaction yields, *E*-Factor and EcoScale values

	E-Factor	EcoScale	Yield (%)
Tris-pyrazole ligand **3a**			
Mechanochemistry (this work)	5.7	51.5	53
Pinho e Melo method[23]	68.4	46.5	87
Copper C-Scorpionate **6a**			
Mechanochemistry (this work)	0.4	72.5	79
Pettinari method[29]	320.8	34.5	43
CuAAC reaction for the synthesis of triazole **13**			
Mechanochemistry (this work)	0.5	46	78
CuAAC reaction for the synthesis of triazole **13**[22]	29.0	35.5	79

The preparation of the copper(II) C-scorpionate complexes under mechanochemical conditions is highly effective, and the use of equimolar amounts of the copper salt and the absence of a solvent led to an almost ideal *E*-factor value (*E*-Factor = 0.4) reflecting the low amount of waste obtained from the reaction and far from that obtained when the method in solution previously described is used to synthesize a similar copper complex (*E*-Factor = 320.8).[29] A high value of EcoScale was also obtained for the complex synthesis under ball milling (72.5), close to the ideal 100 points, which are unachievable mostly due to the inherent toxicity of the copper acetate salt (ESI,† Table S7).

The three-component AAC reaction using copper(II) C-scorpionate complexes as catalysts gave similar yields under mechanochemical action and under microwave irradiation, however, the synthesis of the triazole under ball milling gave an impressive *E*-Factor value of 0.5, an improved performance when compared to the reaction carried out under microwave

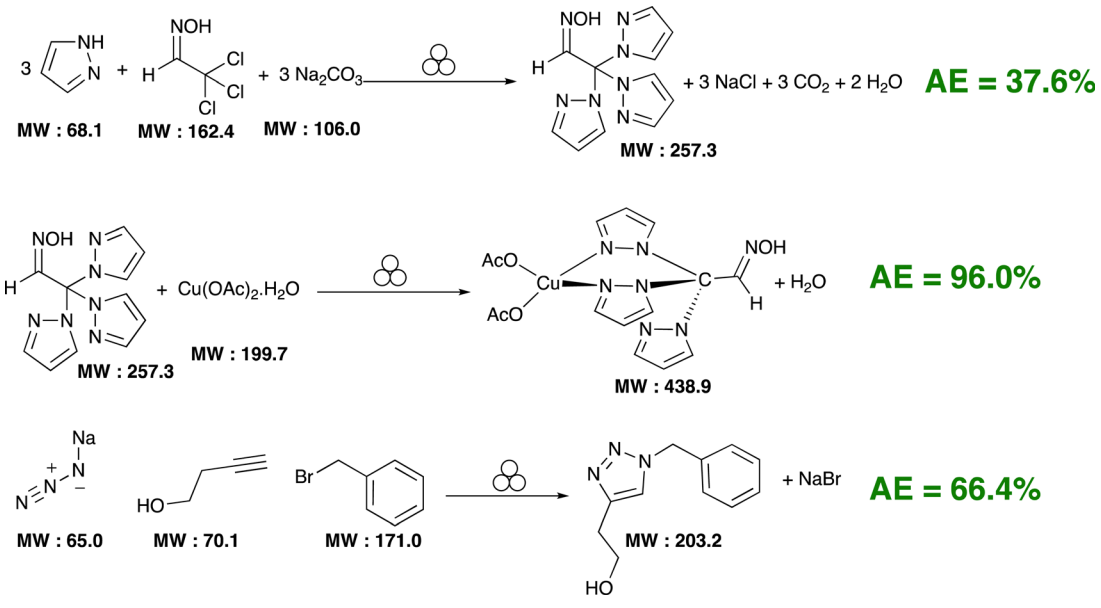

Fig. 6 Atom economy of the chemical transformations in this work.

irradiation (29.0), in which the amount of solvent (MeOH/H_2O) was already greatly reduced. The increase of sustainability using the mechanochemical conditions is also evidenced in the recovery of the EcoScale values from 35.5 to 46 points, reflecting the elimination of the solvent and the formation of sodium bromide as only secondary product (ESI,† Table S8).

Overall, the reported results show that the development of synthetic methods under mechanochemical conditions can reduce the use of reactants in excess, eliminate solvents, and maintain the efficiency of the synthetic process. This reduction in waste generation is reflected in the obtained sustainability metrics.

3. Conclusions

The synthesis of a set of tris(pyrazol-1-yl)methanes and bis(pyrazol-1-yl)methanes bearing an oxime group was successfully obtained *via* the 1,4-conjugated addition of pyrazole to nitrosoalkenes under solvent-free mechanochemistry conditions. These compounds proved to be efficient ligands for the synthesis of novel copper(II) C-scorpionates using only equimolar amounts of the pro-ligand and metal salt. The resulting copper(II) complexes were tested as catalysts for the three-component synthesis of triazoles under ball milling *via* the synthesis of benzyl azide followed by azide–alkyne cycloaddition reactions. Overall, the copper C-scorpionates increased the reaction rate and yield. The structure of the ligand was found to influence the catalytic activity, with those with unsubstituted pyrazole units leading to higher yields of triazole (with aliphatic and aromatic substituents).

Overall, the development of synthetic methods using mechanochemistry in combination with catalysis offers advantages such as reduction of the use of excess reactants, the elimination of solvents and an increase in the efficiency of the catalytic process. These benefits are reflected in the sustainability metrics obtained for the developed processes.

4. Experimental

4.1. Materials and methods

Ball milling reactions were performed in a Retsch MM400 mill by constant monitoring of frequency and time. Stainless steel jars (10 mL) and stainless-steel spheres (7 mm diameter) were used. NMR spectra were registered at room temperature (RT) in a Bruker Advance III spectrometer, operating at 400 MHz. TMS was the internal standard used. Chemical shifts (δ) and coupling constants (J) are indicated in ppm and Hz, respectively. Microwave-assisted reactions were performed in a CEM Discover S-Class single-mode microwave reactor featuring continuous temperature, time, pressure and microwave power monitoring. High-resolution mass spectra (HRMS) were obtained using a TOF VG Autospect M spectrometer with electrospray ionization (ESI), or an Orbitrap Q-Exactive Focus mass spectrometer (Thermo Scientific), coupled to a Vanquish HPLC system (Thermo Scientific), operating in positive or negative ionization mode with electrospray ionization (ESI). The elemental analysis of the compounds was performed using a Vario Micro Cube Elemental Analyzer. The melting points were determined using a Falc device (open glass capillary method).

All commercially acquired reagents were high-grade chemicals and were used without any additional purification: pyrazole (288-13-1, Fluorochem, 99%), 4-methylpyrazole (7554-65-6, Fluorochem, 97%), sodium carbonate anhydrous (497-19-8, Merck, 99%), copper(II) acetate monohydrate (142-71-2, J. T. Baker), sodium azide (26628-22-8, Acros Organics, 99%), benzyl bromide (100-39-0, Alfa Aesar, 99%), 3-butyn-1-ol (927-74-2, Alfa Aesar, 98%), ethynyltrimethylsilane (1066-54-2, Merck, 98%), 1,1-diphenyl-2-propyn-1-ol (3923-52-2, Sigma-Aldrich, 99%), phenylacetylene (536-74-3, Alfa Aesar, 98+%), 4-ethynyltoluene (766-97-2, Sigma-Aldrich, 97%), 3-butyn-2-ol (2028-63-9, Fluorochem, 97%).

4.2. Synthetic procedures

4.2.1. General procedure for the synthesis of tris(pyrazolyl)-methanes. 2,2,2-Trichloroacetaldehyde oxime (3.2 mmol, 0.518 g) and the corresponding pyrazole (3.3 equiv.) were mixed with sodium carbonate (5 equiv., 16 mmol, 1.696 g) in a 10 mL ball milling stainless steel jar for mechanochemistry. Two stainless steel balls (7 mm of diameter) were added and the mixture was subjected to ball milling with a frequency of 25 Hz during 30 min. The solid product was removed using ethyl acetate, filtrated through Celite and the solvent was evaporated under a vacuum.

*(E)-2,2,2-Tris(1H-pyrazol-1-yl)acetaldehyde oxime (**3a**).* The product was purified through flash column chromatography of silica gel using ethyl acetate/hexane (1 : 2) as an eluent. Recrystallization from ethanol/diethyl ether yields the desired product in 52% yield. M_p 143.6–144.3 °C; ^{1}H-NMR (400 MHz, DMSO-d_6), δ (ppm) = 11.98 (1H, sl, HON), 8.64 (1H, s, CH), 7.71 (3H, d, J = 1.6 Hz, CH), 7.40 (3H, d, J = 2.4 Hz, CH), 6.46 (3H, t, J = 2.4 Hz, CH). The characterization is in accordance with that previously described by Pinho e Melo *et al.*[23]

*(E)-2,2,2-Tris(4-methyl-1H-pyrazol-1-yl)acetaldehyde oxime (**3b**).* Yield = 42%; mp 121.8–122.6 °C; ^{1}H-NMR (400 MHz, DMSO-d_6), δ (ppm) = 11.85 (1H, s, HON), 8.51 (1H, s, CH), 7.50 (3H, s, CH), 7.15 (3H, s, CH), 2.01 (9H, s, CH_3); ^{13}C-NMR (100 MHz, DMSO-d_6): δ (ppm) = 144.9, 141.5, 128.8, 116.7, 88.0, 8.5; HRMS (ESI) m/z: calculated for ($C_{14}H_{17}ON_7{}^{23}Na$): ([M + Na]$^+$) 322.13868; found ([M + Na]$^+$) 322.1383.

4.2.2. General procedure for the synthesis of bis-(pyrazolyl)methanes. 2,2-Dihaloketone oxime (3 mmol) and pyrazole (3.3 equiv.) were mixed with sodium carbonate (5 equiv., 16 mmol, 1.696 g) in a 10 mL stainless steel jar for ball milling. Two stainless steel balls (7 mm of diameter) were added and the mixture was underwent ball milling with a frequency of 25 Hz during 30 min. The solid product was removed with ethyl acetate, filtrated through Celite and the solvent was evaporated under a vacuum.

*1,1-Bis(1H-pyrazol-1-yl)propan-2-one oxime (**5a**).* Yield = 28%; ^{1}H-NMR (400 MHz, DMSO-d_6), δ (ppm) = 11.37 (1H, s, HON), 7.83 (2H, d, J = 2.0 Hz, CH), 7.58 (2H, d, J = 1.6 Hz, CH), 7.46 (1H, s, CH), 6.34 (2H, t, J = 2.4 Hz, CH), 1.72 (3H, s, CH_3). Characterization in accordance with previously reported in Pinho e Melo *et al.*[23]

*1-(1-(4-Chlorophenyl)-1H-1,2,3-triazol-4-yl)-2,2-bis(1H-pyrazol-1-yl)ethan-1-one oxime (**5b**).* Yield = 17%; mp 220.0–220.9; IR (ATR) υ 757, 986, 1042, 1228, 1242, 1388, 1500, 2988 cm^{-1}; ^{1}H-NMR (400 MHz, DMSO-d_6), δ (ppm) = 12.71 (1H, s, HON), 9.44 (1H, s, CH), 8.34 (1H, s, CH), 8.05–8.01 (2H, m, Ph), 7.88 (2H, d, 2.4 Hz, CH), 7.65–7.69 (2H, m, Ph), 7.55 (2H, d, J = 1.6 Hz, CH), 6.33–6.34 (2H, m, CH); ^{13}C-NMR (100 MHz, DMSO-d_6): δ (ppm) = 153.2, 141.5, 139.7, 137.0, 135.0, 133.4, 130.5, 129.8, 126.5, 122.4, 106.3, 73.5; HRMS (ESI-TOF) m/z: calculated for ($C_{16}H_{14}ClN_8O$): $(M + H)^+$ 369.0974; found $(M + H)^+$ 369.0964.

4.2.3. General procedure for the synthesis C-scorpionate complexes. The corresponding tris- or bis-pyrazolyl methane (50 mg) and the corresponding metal salt (1 equiv.) were mixed in the stainless steel milling jar (10 mL) and 2 stainless steel balls were added (7 mm diameter). The mixture was subjected to high-speed vibration in a Retsch MM400 mill at 25 Hz for 30 min. At the end of the reaction, the solid was scraped off from the jar using a spatula.

*Copper (II) (E)-2,2,2-tris(1H-pirazol-1-yl)acetaldehyde oxime diacetate (**6a**).* Yield = 86%; mp 151.7–152.6 °C; ESI-MS m/z: calculated for ($C_{13}H_{14}CuN_7O_3$) = $(M\text{-}OAc)^+$ 379.0454, found $(M\text{-}OAc)^+$ 379.0446; elemental analysis calculated for ($C_{15}H_{17}CuN_7O_5 + H_2O$) C: 39.43, H: 4.19, N: 21.46, found C: 38.23, H: 3.54, N: 24.92.

*Copper (II) (E)-2,2,2-tris(1H-pirazol-1-yl)acetaldehyde oxime diacetate (**6a**) obtained in solution following the procedure of Pettinari et al*[29]*.* Yield = 36%; mp 151.9–152.6 °C; elemental analysis calculated for ($C_{13}H_{14}CuN_7O_3 + CH_2Cl_2$) C: 36.69, H: 3.66, N: 24.17, found C:35.56, H: 2.6, N: 25.18.

*Copper (II) (E)-2,2,2-tris(1H-pirazol-1-yl)acetaldehyde oxime dichloride (**6b**).* Yield = 79%; mp 118.9–119.5 °C; ESI-TOF m/z: calculated for ($C_{11}H_{11}CuCl_2N_7O$): $(M)^+$ 389.9698, found $(M)^+$ 390.977; Elemental analysis calculated for ($C_{11}H_{11}CuCl_2N_7O + H_2O$) C: 32.25, H: 3.20, N: 23.93 obtained C: 31.08, H: 2.94, N: 22.9.

*Copper (II) (E)-2,2,2-tris(1H-pirazol-1-yl)acetaldehyde oxime dichloride (**6b**) obtained in solution following the procedure of Pettinari et al*[29]*.* Yield = 79%; mp 118.5–119.0 °C; ESI-TOF m/z: calculated for ($C_{11}H_{11}ClCuN_7O$): $(M - Cl)^+$ 355.0004, obtido $(M - Cl)^+$ 354.9999; elemental analysis calculated for ($C_{11}H_{11}Cl_2CuN_7O + H_2O$) C: 32.25, H: 3.20, N: 23.93, obtained C: 32.46, H: 2.91, N: 24.92.

Copper (II) (E)-2,2,2-tris(4-methyl-1H-pirazol-1-yl)acetaldehyde oxime diacetate (7). Yield = 63%; mp 137.5–137.9 °C; elemental analysis calculated ($C_{16}H_{20}CuN_7O_3 + H_2O$) C: 43.68, H: 5.04, N: 22.29, found C: 42.97, H: 4.33, N: 22.20.

*Copper (II) (E)-2,2,2-bis(1H-pirazol-1-yl)propano-2-one oxime diacetate (**8**).* Yield = 50%; mp 107.7–108.3 °C; elemental analysis calculated ($C_{13}H_{17}CuN_5O_5 + H_2O$) C: 38.20, H: 4.66, N: 20.25, found C: 37.08, H: 3.83, N: 20.62.

*Copper (II) (Z)-1-(1-(4-chlorophenyl)-1H-1,2,3-triazol-4-yl)-2,2-bis(1H-pirazol-1-yl)ethan-1-one oxime diacetate (**9**).* Yield = 60%; mp 154.5–155.2; ESI-MS m/z: calculated for ($C_{16}H_{13}ClCuN_8O$): $(M - 2OAc)^+$ 431.0197, found $(M - 2OAc)^+$ 431.0198; elemental analysis calculated ($C_{16}H_{13}ClCuN_8O + 2CH_2Cl_2$) C: 35.90, H: 2.85, N: 18.61, found C: 35.32, H: 2.59, N: 17.86.

4.2.4. General procedure for the Cu catalyzed cycloaddition reaction. Benzyl bromide (0.436 mmol, 52 μL), the desired alkyne (1.1 equiv.) and sodium azide (1.1 equiv., 0.483 mmol, 31.4 mg) and the catalyst (1.5 mol%) were placed in the stainless steel jar for ball milling. Two stainless steel balls (7 mm of diameter) were added and the mixture was subjected to ball milling with a frequency of 30 Hz during 3 h. Triazoles are purified by flash column chromatography using **(13)** ethyl acetate/methanol (97.5 : 2.5 v/v), **(14)** ethyl acetate/*n*-hexane (1 : 3 to 2 : 3 v/v), **(15)** ethyl acetate/*n*-hexane (1 : 2 v/v), **(16)** ethyl acetate/*n*-hexane (1 : 3 v/v), **(17)** ethyl acetate/*n*-hexane (1 : 3 v/v), **(18)** ethyl acetate/*n*-hexane (3 : 1 v/v) to ethyl acetate/methanol (95 : 5 v/v).

*2-(1-Benzyl-1H-1,2,3-triazol-4-yl)ethanol (**13**).* Yield = 78%; ^{1}H-NMR (400 MHz, $CDCl_3$), δ (ppm) = 7.39–7.34 (4H, m, H_{Ph} + $H_{triazole}$), 7.28–7.24 (2H, m, H_{Ph}), 5.48 (2H, s, CH_2), 3.89 (2H, t, J = 5.6 Hz, CH_2), 2.90 (2H, t, J = 6.0 Hz, CH_2), 2.28 (1H, sl, OH). Characterization in accordance with that previously reported by Appukkuttan *et al.*[39]

*1-Benzyl-4-(trimethylsilyl)-1H-1,2,3-triazole (**14**).* Yield = 59%; ^{1}H-NMR (400 MHz, DMSO-d_6), δ (ppm) = 7.41 (1H, s, $H_{triazole}$), 7.40–7.35 (3H, m, H_{Ph}), 7.28 (2H, m, H_{Ph}), 5.56 (2H, s, CH_2), 0.29 (9H, s, CH_3). Characterization in accordance with that previously reported by Appukkuttan *et al.*[39]

*(1-Benzyl-1H-1,2,3-triazol-4-yl)diphenylmethanol (**15**).* Yield = 55%; ^{1}H-NMR (400 MHz, $CDCl_3$), δ (ppm) = 7.37–7.23 (15H, m, H_{Ph}), 7.07 (1H, s, $H_{triazole}$), 5.50 (2H, s, CH_2), 3.69 (1H, s, OH). Characterization in accordance with that previously reported by García-Álvarez *et al.*[40]

*1-Benzyl-4-phenyl-1H-1,2,3-triazole (**16**).* Yield = 19%; ^{1}H-NMR (400 MHz, $CDCl_3$), δ (ppm) = 7.81–7.79 (2H, m, H_{Ph}), 7.65 (1H, s, $H_{triazole}$), 7.42–7.36 (5H, m, H_{Ph}), 7.37–7.31 (3H, m, H_{Ph}), 5.55(2H, s, CH_2). Characterization in accordance with that previously reported by Ozkal *et al.*[41]

*1-Benzyl-4-(p-tolyl)-1H-1,2,3-triazole (**17**).* Yield = 68%; ^{1}H-NMR (400 MHz, $CDCl_3$), δ (ppm) = 7.71 (2H, d, J_1 = 8 Hz, H_{Ph}), 7.64 (1H, s, $H_{triazole}$), 7.42–7.40 (3H, m, H_{Ph}), 7.35–7.32 (2H, m, H_{Ph}), 7.23 (3H, d, J = 7.6 Hz, H_{Ph}) 5.57 (2H, s, CH_2), 2.37 (3H, s, CH_3). Characterization in accordance with that previously reported by Liu *et al.*[42]

*1-(1-Benzyl-1H-1,2,3-triazol-4-yl)ethan-1-ol (**18**).* Yield = 69%; ^{1}H-NMR (400 MHz, $CDCl_3$), δ (ppm) = 7.41 (1H, s, $H_{triazole}$),

7.36–7.35 (3H, m, H_{Ph}), 7.28–7.26(2H, m, H_{Ph}), 5.49 (2H, s, CH_2), 5.04 (1H, q, J = 6.4 Hz, CH), 1.54 (3H, d, J = 6.4 Hz). Characterization in accordance with that previously reported by Sarmiento-Sanchez *et al.*[43]

4.3. X-ray crystallography

Single crystal X-ray diffraction (XRD) measurements were performed at room temperature on a Bruker APEX II diffractometer equipped with a 4K CCD detector, using graphite monochromated MoKα (λ = 0.71073 Å) radiation. A total of 114886 reflections were measured up to θ = 27.5° (R_σ = 0.0109, R_{int} = 0.0467). Integration and correction for Lorentz and polarization were performed using SAINT V8.38A[44] included in the APEXIII package.[45] Absorption corrections, including odd and even spherical harmonics up to rank 3 and 6, respectively, were performed using SADABS-2016/2.[46] The structure was solved by the dual-space algorithm implemented in SHELXT-2018/2,[47] and the refinement of the structural model was performed using full-matrix least-squares method employing SHELXL-2018/3.[48] All non-hydrogen atoms were refined anisotropically. Hydrogen atoms were placed at calculated idealized positions and refined as riding using SHELXL-2018/3 default values, except for that of the hydroxyl group, which is strongly involved in hydrogen-bonding and was refined isotropically. The final quality factors of the refinement were $R_1(I > 2\sigma)$ = 0.0353, wR_{all} = 0.0975 and GOF = 1.035 for 2792 independent reflections and 175 refined parameters. Full details of the data collection and structure refinement procedures are provided in the ESI† (Crystallographic Data). The CIF files containing the supplementary crystallographic data for compound **3a** were deposited at the Cambridge Crystallographic Data Centre, with the reference 2096452.†

4.4. Raman and infrared spectroscopies

The Raman spectra were obtained in a Raman Horiba LabRam HR Evolution system, with excitation at λ = 532 nm, provided by a solid-state laser (laser power $<$5 mW, to prevent the photodegradation of the samples). The spot diameter of the laser was approximately 1 μm, which was focused on the sample using a 50× long-working-distance objective. The final spectra were the average of 1000 to 5000 accumulations of individual spectra collected during 1 to 5 seconds, with the spectral resolution of 0.5 cm^{-1}. The calibration of the system was performed using the silicon crystal Raman peak at 520.5 cm^{-1} as a reference. The infrared spectra were obtained using an Agilent Technologies Cary 630 FTIR spectrophotometer, using the attenuated total reflection (ATR) method.

4.5. Computational details

The computational calculations performed to investigate the optimized geometries and the vibrational spectra of the studied compound were performed within the density functional theory (DFT) framework, using the Gaussian 09 program (Revision A.02).[49] The three-parameter B3LYP density functional, which includes the Becke's gradient exchange correction[50] and the Lee, Yang and Parr correlation functional,[51] together with the 6-311++G(d,p) basis set,[52] was employed in the calculations. All the spectra presented were corrected using the empirical scaling factor value of 0.977.

Author contributions

Carla Gomes: investigation – experimental; writing original draft; Mariana Costa: investigation – experimental; Susana M. M. Lopes: investigation – experimental; Bernardo Albuquerque Nogueira: investigation – experimental; writing original draft; Rui Fausto: investigation (data analysis); writing – review and editing; supervision; José A. Paixão, investigation – experimental; writing; Teresa M. V. D. Pinho e Melo: review and editing; Luísa M. D. R. S. Martins: conceptualization, review and editing; supervision; Marta Pineiro: conceptualization, writing – review and editing; supervision.

Conflicts of interest

There are no conflicts to declare.

Acknowledgements

The authors thank CQC-IMS and CFisUC supported by the Portuguese Agency for Scientific Research, ''Fundação para a Ciência e a Tecnologia'' (FCT) through projects UIDB/00313/2020 and UIDP/00313/2020, UIDB/04564/2020 and UIDP/04564/2020, co-funded by COMPETE2020-UE. This work was also supported by Project PTDC/QUI-QOR/0103/2021, funded by national funds (PIDDAC). Centro de Química Estrutural (CQE) acknowledges support through the UIDB/00100/2020 and UIDP/00100/2020 projects, and the Institute of Molecular Sciences (IMS) through the project LA/P/0056/2020 of FCT. C. G. acknowledges the financial support from the PhD fellowship (FCT-PD/BD/135531/2018) of the FCT Doctoral Program ''Catalysis and Sustainability'' CATSUS (PD/00248/2012). We also acknowledge the LaserLab Coimbra and the UC-NMR (www.nmrccc.uc.pt) facilities for making available the instrumentation for IR/Raman and NMR experiments, respectively.

References

1 K. J. Ardila-Fierro and J. G. Hernández, *ChemSusChem*, 2021, **14**, 2145–2162.
2 N. Nebra and J. García-Álvarez, *Molecules*, 2020, **25**, 2015.
3 M. Trujillo, C. Hull-Crew, A. Outlaw, K. Stewart, L. Taylor, L. George, A. Duensing, B. Tracey and A. Schoffstall, *Molecules*, 2019, **24**, 973.
4 A. K. Agrahari, P. Bose, M. K. Jaiswal, S. Rajkhowa, A. S. Singh, S. Hotha, N. Mishra and V. K. Tiwari, *Chem. Rev.*, 2021, **121**, 7638–7956.
5 S. Neumann, M. Biewend, S. Rana and W. H. Binder, *Macromol. Rapid Commun.*, 2020, **41**, 1900359.
6 N. Aflak, H. B. El Ayouchia, L. Bahsis, H. Anane, M. Julve and S.-E. Stiriba, *Int. J. Mol. Sci.*, 2022, **23**, 2383.

7 H. C. Kolb, M. G. Finn and K. B. Sharpless, *Angew. Chem., Int. Ed.*, 2001, **40**, 2004–2021.
8 D. Castelvecchi and H. Ledford, *Nature*, 2022, **610**, 242–243.
9 R. Thorwirth, A. Stolle, B. Ondruschka, A. Wildb and U. S. Schubertb, *Chem. Commun.*, 2011, **47**, 4370–4372.
10 M. Tireli, S. Maračić, S. Lukin, M. J. Kulcsár, D. Žilić, M. Cetina, I. Halasz, S. Raić-Malić and K. Užarević, *Beilstein J. Org. Chem.*, 2017, **13**, 2352–2363.
11 L. Rinaldi, K. Martina, F. Baricco, L. Rotolo and G. Cravotto, *Molecules*, 2015, **20**, 2837–2849.
12 T. L. Cook, J. A. Walker and J. Mack, *Green Chem.*, 2013, **15**, 617–619.
13 M. Tyagi, N. Taxak, P. V. Bharatam, H. Nandanwar and K. P. R. Kartha, *Carbohydr. Res.*, 2015, **407**, 137–147.
14 N. Rubio, K.-C. Mei, R. Klippstein, P. M. Costa, N. Hodgins, J. T.-W. Wang, F. Festy, V. Abbate, R. C. Hider, K. L. A. Chan and K. T. Al-Jamal, *ACS Appl. Mater. Interfaces*, 2015, **7**, 18920–18923.
15 A. Otero, J. Fernández-Baeza, A. Lara-Sánchez and L. F. Sánchez-Barba, *Coord. Chem. Rev.*, 2013, **257**, 1806–1868.
16 L. M. D. R. S. Martins and A. J. L. Pombeiro, *Coord. Chem. Rev.*, 2014, **265**, 74–88.
17 L. M. D. R. S. Martins, *Coord. Chem. Rev.*, 2019, **396**, 89–102.
18 J. M. Muñoz-Molina, T. R. Belderrain and P. J. Pérez, *Coord. Chem. Rev.*, 2019, **390**, 171–189.
19 C. Pettinari, R. Pettinari and F. Marchetti, *Adv. Organom. Chem.*, 2016, 175–260.
20 C. J. Carrano, *Eur. J. Inorg. Chem.*, 2016, 2377–2390.
21 I. Cano, M. C. Nicasio and P. J. Pérez, *Org. Biomol. Chem.*, 2010, **8**, 536–538.
22 A. G. Mahmoud, L. M. D. R. S. Martins, M. F. C. Guedes da Silva and A. J. L. Pombeiro, *Inorg. Chim. Acta*, 2018, **483**, 371–378.
23 T. M. V. D. Pinho e Melo, A. Lemos and C. Grosso, *Synlett*, 2014, 2868–2872.
24 *Eur-Lex Acess to European Union Law*, 2023, **https://eur-lex.europa.eu/eli/dir/1999/13/oj**.
25 S. M. M. Lopes, A. L. Cardoso, A. Lemos and T. M. V. D. Pinho e Melo, *Chem. Rev.*, 2018, **118**, 11324–11352.
26 I. Cortes and A. M. Sarotti, *Org. Biomol. Chem.*, 2023, **21**, 2935–2940.
27 N. A. M. Pereira, S. M. M. Lopes, A. Lemos and T. M. V. D. Pinho e Melo, *Synlett*, 2014, **25**, 423–427.
28 S. M. M. Lopes, J. S. Novais, D. C. S. Costa, H. C. Castro, A. M. S. Figueiredo, V. F. Ferreira, T. M. V. D. Pinho e Melo and F. Carbalho da Silva, *Eur. J. Med. Chem.*, 2018, **143**, 1010–1020.
29 D. Martini, M. Pellei, C. Pettinari, B. W. Skelton and A. H. White, *Inorg. Chim. Acta*, 2002, **333**, 72–82.
30 B. H. M. Kuijpers, S. Groothuys, A. R. Keereweer, P. J. L. M. Quaedflieg, R. H. Blaauw, F. L. van Delft and F. P. J. T. Rutjes, *Org. Lett.*, 2004, **6**, 3123–3126.
31 W. S. Brotherton, H. A. Michaels, J. T. Simmons, R. J. Clark, N. S. Dalal and L. Zhu, *Org. Lett.*, 2009, **11**, 4954–4957.
32 G.-C. Kuang, H. A. Michaels, J. T. Simmons, R. J. Clark and L. Zhu, *J. Org. Chem.*, 2010, **75**, 6540–6548.
33 K. R. Reddy, K. Rajgopal and M. L. Kantam, *Synlett*, 2006, 957–959.
34 *Bordwell pKa Table*, 2023, **https://organicchemistrydata.org/hansreich/resources/pka/**.
35 L. Jin, E. A. Romero, M. Melaimi and G. Bertrand, *J. Am. Chem. Soc.*, 2015, **137**, 15696–15698.
36 B. M. Trost, *Acc. Chem. Res.*, 2002, **35**, 695–705.
37 R. A. Sheldon, *Green Chem.*, 2017, **19**, 18–43.
38 K. Van Aken, L. Strekowski and L. Patiny, *Beilstein J. Org. Chem.*, 2006, **2**, 1–7.
39 P. Appukkuttan, W. Dehaen, V. V. Fokin and E. Van der Eycken, *Org. Lett.*, 2004, **6**, 4223–4225.
40 J. García-Álvarez, J. Díez and J. Gimeno, *Green Chem.*, 2010, **12**, 2127–2130.
41 E. Ozkal, S. Özçubukçu, C. Jimeno and M. A. Pericàs, *Catal. Sci. Technol.*, 2012, **2**, 195–200.
42 J. Liu, M. Liu, Y. Yue, M. Yao and K. Zhuo, *Chin. J. Chem.*, 2012, **30**, 644–650.
43 J. I. Sarmiento-Sanchez, A. Ochoa-Teran and I. A. Rivero, *ARKIVOC*, 2011, **IX**, 177–188.
44 Bruker, *SAINT V8.38A*, Bruker AXS Inc., Madison, Wisconsin, USA, 2016.
45 Bruker, *APEX3*, Bruker AXS Inc., Madison, Wisconsin, USA, 2016.
46 L. Krause, R. Herbst-Irmer, G. M. Sheldrick and D. Stalke, *J. Appl. Cryst.*, 2015, **48**, 3–10.
47 G. M. Sheldrick, *Acta Cryst. A*, 2015, **71**, 3–8.
48 G. M. Sheldrick, *Acta Cryst. C*, 2015, **71**, 3–8.
49 M. J. Frisch, G. W. Trucks, H. B. Schlegel, G. E. Scuseria, M. A. Robb, J. R. Cheeseman, G. Scalmani, V. Barone, B. Mennucci, G. A. Petersson, H. Nakatsuji, M. Caricato, X. Li, H. P. Hratchian, A. F. Izmaylov, J. Bloino, G. Zheng, J. L. Sonnenberg, M. Hada, M. Ehara, K. Toyota, R. Fukuda, J. Hasegawa, M. Ishida, T. Nakajima, Y. Honda, O. Kitao, H. Nakai, T. Vreven, J. A. Montgomery, Jr., J. E. Peralta, F. Ogliaro, M. Bearpark, J. J. Heyd, E. Brothers, K. N. Kudin, V. N. Staroverov, R. Kobayashi, J. Normand, K. Raghavachari, A. Rendell, J. C. Burant, S. S. Iyengar, J. Tomasi, M. Cossi, N. Rega, J. M. Millam, M. Klene, J. E. Knox, J. B. Cross, V. Bakken, C. Adamo, J. Jaramillo, R. Gomperts, R. E. Stratmann, O. Yazyev, A. J. Austin, R. Cammi, C. Pomelli, J. W. Ochterski, R. L. Martin, K. Morokuma, V. G. Zakrzewski, G. A. Voth, P. Salvador, J. J. Dannenberg, S. Dapprich, A. D. Daniels, O. Farkas, J. B. Foresman, J. V. Ortiz, J. Cioslowski and D. J. Fox, *Gaussian 09*, Gaussian, Inc., Wallingford CT, 2009.
50 A. D. Becke, *Phys. Rev. A: At., Mol., Opt. Phys.*, 1988, **38**, 3098–3100.
51 C. Lee, W. Yang and R. G. Parr, *Phys. Rev. B: Condens. Matter Mater. Phys.*, 1988, **37**, 785–789.
52 A. D. McLean and G. S. Chandler, *J. Chem. Phys.*, 1980, **72**, 5639.

